Hydroamination on Homogeneous and Heterogeneous Catalysts: Kinetic Study

Thomas E. Müller and Johannes A. Lercher
Lehrstuhl II für Technische Chemie, Technische Universität München, 85747 Garching, Germany

Nguyen Van Nhu
Lehrstuhl für Technische Thermodynamik, RWTH-Aachen, 52056 Aachen, Germany

This kinetic analysis compares homogeneous and heterogeneous catalysts for the cyclization of 6-aminohex-1-yne. The reaction was studied as a model for the direct addition of amine N–H bonds to CC multiple bonds (hydroamination). Kinetic modeling showed that the metal-catalyzed hydroamination reaction is followed by a proton-catalyzed isomerization of the primary reaction product, 2-methylene-piperidine, to the thermodynamically more stable 2-methyl-1,2-dehydropiperidine.

Introduction

The direct reaction of alkenes and alkynes with N–H bonds (hydroamination) is a highly attractive route for the synthesis of nitrogen-containing compounds (Müller and Beller, 1998; Roundhill, 1992). One challenge in developing appropriate catalyst systems for such reactions is that their thermodynamic driving force is low, and an equilibrium condition may be reached rather than a complete conversion (Koch et al., 1999). Commercially, *tert*-butylamine was the first amine produced on a large scale by this route by BASF (Tanabe and Hölderich, 1999). Ammonia and *iso*-butene are reacted at 300°C and 300 bar to achieve a maximum conversion of 12–15% (Hölderich and Heitmann, 1997). Thus, more than 85% of the starting material has to be recycled, which is a costly factor in technical synthesis. With a more active catalyst system, the reaction temperature could be lowered and a higher conversion achieved. Even more advanced catalyst systems are required for the conversion of alkenes, which are less reactive than *iso*-butene. The corresponding addition of N–H bonds to alkynes is thermodynamically more favorable, but the thermal lability of the primary and secondary reaction products, enamines and imines, respectively, requires as low a reaction temperature as possible.

Several different catalyst systems are known for the direct addition of amine N–H bonds to CC double and triple bonds:

1. The commercial process utilizes solid acids, such as H-BEA-zeolite, that are able to protonate the *iso*-butene to the corresponding *tert*-butyl carbenium ion (Lequitte et al., 1996; Mizuno et al., 1994). The latter then reacts with ammonia. The drawback of solid acid catalysts is that their use is restricted to those alkenes that form relatively stable alkoxy groups. Another technique is to immobilize metal cations on a solid. The possibility of catalyzing hydroamination reactions with such catalysts has been demonstrated for Zn^{2+} ion exchanged zeolites in the addition of methylamine to propyne (Neale et al., 1972) and the cyclization of 6-aminohex-1-yne (Penzien et al., 2000, 2001).

2. Homogeneous catalysts are based either on early transition metal complexes, such as $[(C_5Me_5)_2SmNH(SiMe_3)_2]$, C_5Me_5 = pentamethylcyclopentadienyl (Li and Marks, 1996), or late transition metal complexes, such as [Pd(Triphos)]-$(CF_3SO_3)_2$, Triphos = *bis*-(2-diphenylphosphinoethyl)-phenylphosphane (Müller and Pleier, 1998; Müller et al., 2000). Complexes based on the late transition metals have a much higher tolerance to water and oxygen impurities and are, thus, of more interest for applications. However, separating the product phase from a therein soluble (molecular) catalyst is often a major challenge. Thermal separation rarely leads to quantitative recovery of the catalyst and normally induces thermal stress on the catalyst, resulting in progressive degradation.

3. Liquid–liquid two-phase catalysis combines the advantages of homogeneous catalysts (high activity and high selectivity) with a simple and complete separation of the product from the catalyst. Examples are the cyclization of *o*-ethynylaniline with palladium(II)-salts, which can be achieved in a two-phase system comprising CH_2Cl_2 and aqueous HCl (Cacchi et al., 1994) and the cyclization of 6-aminohex-1-yne with $Zn(CF_3SO_3)_2$ in a two-phase system comprising heptane and an ionic liquid (Neff et al., 2002).

In order to decide which of the different strategies gives the best performance in technical applications, the microki-

Correspondence concerning this article should be addressed to T. E. Müller.

netics of the reaction have to be directly compared. In this study, the cyclization of 6-aminohex-1-yne was chosen as a model reaction for the direct addition of N–H bonds to unsaturated carbon–carbon bonds. For the first time, we report an extensive kinetic study on the catalytic activity of homogeneous catalysts [that is, $Zn(CF_3SO_3)_2$] in comparison to suspended heterogeneous catalysts (Zn^{2+} ion exchanged zeolites).

Experimental

All commercially available compounds were used as received. Solvents were obtained dry from Aldrich Co. The preparation of 6-aminohex-1-yne and $[Pd(Triphos)](CF_3SO_3)_2$ was performed using standard Schlenk techniques. ^1H-, $^{13}C\{^1H\}$-, and $^{31}P\{^1H\}$-NMR spectra were recorded on a Bruker AM 400 and referenced in ppm relative to tetramethylsilane with the solvent shift as the internal standard (Gottlieb et al., 1997). GC-analyses were performed on a HP 5890A gas chromatograph equipped with a crosslinked 5% diphenyl-95% dimethyl-polysiloxane column (30 m, Restek GmbH, Rtx-5 Amine). Infrared spectra were obtained on a Perkin-Elmer 2000 FT-IR spectrometer. Mass spectroscopic analyses were performed on a Finnigan MAT 311A by chemical ionization (CI) or the fast atom bombardment (FAB) method. Elemental analyses were performed by the Microanalytical Laboratory of the Technische Universität München.

Preparation of 6-Aminohex-1-yne

The compound 5-cyanopent-1-yne (25.0 g, 0.269 mol) was dissolved in Et_2O (100 cm^3) and added over a period of 60 min to a magnetically stirred mixture of $LiAlH_4$ (11.0 g, 0.289 mol) in Et_2O (400 cm^3) at 0°C. The mixture was refluxed overnight, the excess $LiAlH_4$ destroyed by the addition of H_2O (75 cm^3), the mixture filtered, and the organic layer separated. The Et_2O was removed to yield a yellow liquid. The addition of HCl (1 M in Et_2O, 300 cm^3, 0.300 mol) precipitated the product as the hydrochloride, which was filtered off and dried in a vacuum. The hydrochloride (23.3 g) was dissolved in methanol (100 cm^3), Na_2CO_3 (18.5 g, 0.175 mol) added, and the mixture stirred at room temperature for 1 h. The solvent was removed and the product distilled (69–70°C at 18 mm).

Yield: 10.6 g, 41%. Found: C, 74.3; H, 11.4; N, 14.2%. Calc. for $C_6H_{11}N$: C, 74.2; H, 11.3; N, 14.4%. d : 0.852 $g \cdot cm^{-3}$. $^{13}C\{^1H\}$ NMR ($CDCl_3$) : δ 84.3 (s, C2), 68.4 (s, C1), 41.7 (s, C6), 32.8 (s, C5), 25.8 (s, C4), 18.3 (s, C3). ^1H NMR ($CDCl_3$) : δ 2.72 (t, 2H, CH_2-N), 2.22 (td, 2H, CH_2-C $\equiv$ C), 1.96 (t, 1H, HC $\equiv$ C), variable 1.9 – 1.6 (m, 2H, NH_2), 1.57 (m, 4H, CH_2-CH_2). m/z (CI) 98 ($M^+ + 1$). IR (film): 3295 (vs), 2934 (vs), 2862 (s), 2115 (m), 1596 (s), 1455 (s), 1392 (w), 1328 (w), 1037 (s), 943 (w), 896 (w) 635 (s) cm^{-1}.

Preparation of $[Pd(Triphos)](CF_3SO_3)_2$

The complex $[PdCl_2(cod)]$, cod = 1,5-cyclooctadiene, (0.38 g, 1.3 mmol) was dissolved in CH_2Cl_2 (90 cm^3) at 30°C and a solution of *bis*-(2-diphenylphosphinoethyl)-phenylphosphine (Triphos, 0.71 g, 1.3 mmol) in CH_2Cl_2 (15 cm^3) added. The volume was reduced in a partial vacuum to about 5 cm^3. The addition of pentane yielded a yellowish precipitate of [PdCl(Triphos)]Cl, which was recrystallized from CH_2Cl_2/pentane and dried in a vacuum.

Yield: 0.86 g, 91%. Found: C, 54.5; H, 4.3%. Calc. for $C_{34.5}H_{34}Cl_3P_3Pd$: C, 54.9; H, 4.5%. $^{31}P\{^1H\}$-NMR ($CDCl_3$): 110.9 (s, 1P, PPh), 45.5 (s, 2P, PPh_2). $^{13}C\{^1H\}$-NMR ($CDCl_3$): 134.5 – 125.0 (mm, Ph), 29.6 (d, CH_2), 28.6 (m, CH_2). ^1H-NMR ($CDCl_3$): 8.24 (dd, 2H, Ph), 7.85 (quart, 4H, Ph), 7.70 (quart, 4H, Ph), 7.60 – 7.44 (mm, 15H, Ph), 5.73 (b, 1H, CH_2Cl_2), 3.87 (sept, 2H, CH_a), 3.14 (dd, $^2J(^1H, ^{31}P)$ 58 Hz, $^3J(^1H, ^{31}P)$ 12 Hz, $CH_{a'}$), 2.75 (b, 2H, CH_b), 2.23 (b, 2H, $CH_{b'}$). IR (KBr): 3049 (m), 2890 (m), 2806 (w), 1483 (s), 1435 (vs), 1411 (s), 1308 (w), 1189 (w), 1102 (vs), 998 (s), 827 (s), 746 (s), 725 (s), 708 (s), 689 (vs), 656 (m) cm^{-1}. m/z (FAB) 677 (M^+-Cl).

The complex [PdCl(Triphos)]Cl (0.10 g, 0.14 mmol) was dissolved in CH_2Cl_2 (10 cm^3), a solution of $AgCF_3SO_3$ (72 mg, 0.28 mmol) in CH_3CN (2 cm^3) added, and the mixture stirred at RT overnight. A white precipitate formed was removed by filtration. The volume of the filtrate was reduced in a partial vacuum. Addition of Et_2O yielded a light yellow solid, which was recrystallized from CH_2Cl_2/pentane and dried in a vacuum.

Yield: 0.11 g, 85%. Found: C, 46.2; H, 3.5%. Calc. for $C_{36}H_{33}F_6O_6P_3PdS_2$: C, 46.2; H, 3.5%. $^{31}P\{^1H\}$-NMR ($CDCl_3$): 115.1 (s, 1P, PPh), 52.0 (s, 2P, PPh_2). $^{13}C\{^1H\}$-NMR ($CDCl_3$): 134.7 to 123.9 (mm, Ph), 29.8 (d, $^1J(^{13}C, ^{31}P)$ 35 Hz, CH_2), 28.4 (t, $^{1/3}J(^{13}C, ^{31}P)$ 17 Hz, CH_2). ^1H-NMR ($CDCl_3$): 8.19 (dd, 2H, Ph), 7.74 – 7.48 (mm, 23H, Ph), 3.37 (sept, 2H, CH_a), 3.11 (dd, $^2J(^1H, ^{31}P)$ 55 Hz, $^3J(^1H, ^{31}P)$ 15 Hz, $CH_{a'}$), 3.00 (m, 2H, CH_b), 2.25 (b, 2H, $CH_{b'}$). IR (KBr): 3058 (m), 2965 (w), 2920 (w), 1485 (m), 1437 (s), 1324 (m), 1266 (vs), 1158 (s), 1105 (s), 1030 (vs), 999 (m), 830 (m), 747 (m), 725 (m), 709 (m), 690 (m), 637 (vs), 572 (m) cm^{-1}. m/z (FAB) 789 (M^+-CF_3SO_3), 640 (M^+-$2CF_3SO_3$).

Preparation of zeolite Zn/H-BEA

The Zn^{2+} ion exchanged zeolite was prepared by slurrying H-BEA zeolite (Südchemie AG, T-4546, MA039 H/99, 10 g) with 0.06 M zinc acetate in water (100 cm^3) at 80°C and separated subsequently by centrifugation. The procedure was repeated three times to ensure complete ion exchange. Finally, the sample was calcined (5 K/min to 500°C, 8 h at 500°C). The zinc loading was determined by atomic absorption spectroscopy (0.03 g Zn^{2+}, 0.49 mmol Zn^{2+} per gram zeolite). The BET surface areas of the material were 536 and 494 m^2/g before and after the ion exchange, respectively.

Catalysis

All reactions were carried out in custom-built 100- or 120-cm^3 steel autoclaves (Van Nhu et al., 2001). Both reactors were equipped with quartz probes for *on-line* UV- and NIR-spectroscopy. The probes were connected with optical fibers to a Perkin-Elmer Lambda 16 UV- and a Bruker Vector 22/N NIR-spectrometer, respectively.

All kinetic measurements were performed according to the following procedure: A solution of the catalyst in the appropriate solvent was introduced into the reactor. The mixture was stirred and heated to the desired temperature. The reaction was then started by introducing a solution of the substrate from a sample loop with a known volume into the reac-

tor. The amount of catalyst and 6-aminohex-1-yne, the solvent, and the reaction conditions employed in the experiments are summarized in Table 1.

The program OPUS was used to analyze the spectra (OPUS, 2000). After base-line correction (NIR), the spectra were integrated in the following frequency ranges: NIR-spectroscopy 6,360 to 6,660 cm^{-1} for (1+2), 5,190 to 5,370 cm^{-1} for (2+3), 4,830 to 5,070 cm^{-1} for (1); UV-spectroscopy 220 to 370 nm for (3). The parameters α, β, and k of the model (see text below) were then fitted to the experimentally determined concentrations using the solver module of Excel (Arena and Leu, 1999). The fitting routine is described in the Appendix.

Results and Discussion

In situ spectroscopy

The activity of various catalytic systems was compared for the cyclization of 6-aminohex-1-yne (1). The cyclization of 1 first generates 2-methylene-piperidine (2) with an exocyclic double bond (Eq. 1). A subsequent 1,3-hydrogen shift occurs *in situ* and converts the enamine to the more stable isomeric imine 2-methyl-1,2-dehydropiperidine (3)

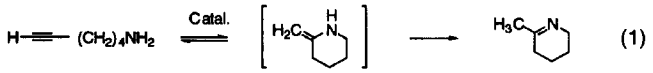

(1)

1 2 3

The reaction was performed in toluene or CH_3CN, and the concentration of the reactants and products followed *in situ* with UV- or NIR-spectroscopy. Toluene was chosen as it had been described as a good solvent for hydroamination reactions (Müller et al., 2000). However, toluene showed a strong absorption in the UV region, and the reaction could, thus, only be followed with NIR-spectroscopy. As a solvent, which had a large spectroscopic window for UV- and NIR-spectroscopy (Marcus, 1999), CH_3CN was chosen. Acetonitrile had an absorption maximum in the UV region at 190 nm due to the $C \equiv N\ \pi \rightarrow \pi^*$ transition, whereas at wavelengths $\geq$200 nm, the absorption was negligible. The substrate 1 had an absorption maximum at 208 nm (due to the C–N $n \rightarrow \sigma^*$ transition) with a weak shoulder extending to 320 nm. The product 3 had an absorption maximum at 220 nm (due to the $C = N\ \pi \rightarrow \pi^*$ transition) and an additional absorption maximum at 305 nm (due to the $C = N\ n \rightarrow \pi^*$ transition). The latter absorption maximum was used to follow the concentration of the product with UV spectroscopy, performing the quantitative analysis of (3) in the 220–370 nm region.

When the cyclization of 1 was performed in CH_3CN and followed with NIR-spectroscopy, bands with a decreasing intensity were observed at 6,512 (m) and 4,955 (m) cm^{-1} and bands with an increasing intensity at 7,348 (w), 7,237 (w), 7,109 (m) and 5,264 (w) cm^{-1}. The band at 4,955 cm^{-1} is characteristic of the N–H stretch vibration of primary amines (Buback and Vögele, 1993) and can, thus, be assigned to 1. For the quantitative analysis, the region 4,830–5,070 cm^{-1} proved suitable.

Figure 1 shows the change in concentration of substrate 1 and product 3 as obtained from NIR- and UV-spectroscopy, respectively. Initially, the concentration of 1 decreased rapidly, whereas 3 was formed with a time delay. At longer reaction times, the concentration of 3 increased, but always

Table 1. Reaction Conditions Employed in the Experiments

Catalyst	(mg)	6-Aminohex-1-yne (mmol)	6-Aminohex-1-yne (μL)	6-Aminohex-1-yne (mmol)	Solvent	(cm^3)	Temp. (°C)
$[Cu(CH_3CN)_4]PF_6$	8.3	0.02	25	0.22	CH_3CN	80	82
$[Cu(CH_3CN)_4]PF_6$	8.3	0.02	25	0.22	CH_3CN	80	100
$[Cu(CH_3CN)_4]PF_6$	6.9	0.02	21	0.18	CH_3CN	80	110
$[Cu(CH_3CN)_4]PF_6$	8.3	0.02	25	0.22	CH_3CN	80	120
$[Pd(CH_3CN)_4](BF_4)_2$	17.9	0.04	45	0.40	CH_3CN	50	82
$[Pd(CH_3CN)_4](BF_4)_2$	20.6	0.05	52	0.46	CH_3CN	50	100
$[Pd(CH_3CN)_4](BF_4)_2$	19.7	0.04	50	0.44	CH_3CN	50	120
$[Pd(Triphos)](CF_3SO_3)_2$	14.2	0.02	169	1.51	CH_3CN	60	82
$[Pd(Triphos)](CF_3SO_3)_2$	13.5	0.01	161	1.43	CH_3CN	60	100
$[Pd(Triphos)](CF_3SO_3)_2$	6.1	0.01	73	0.65	CH_3CN	48	120
$[Pd(Triphos)](CF_3SO_3)_2$	19.6	0.02	237	2.08	Toluene	59	111
$Zn(CF_3SO_3)_2$	70.1	0.19	216	1.93	CH_3CN	60	82
$Zn(CF_3SO_3)_2$	8.5	0.02	263	2.35	CH_3CN	60	82
$Zn(CF_3SO_3)_2$*	14.4	0.04	443	3.95	CH_3CN	58	82
$Zn(CF_3SO_3)_2$	17.2	0.05	50	0.47	CH_3CN	60	100
$Zn(CF_3SO_3)_2$	13.0	0.04	40	0.36	CH_3CN	80	110
$Zn(CF_3SO_3)_2$	8.2	0.02	25	0.22	CH_3CN	80	120
$Zn(CF_3SO_3)_2$	14.9	0.04	458	4.10	Toluene	70	82
$Zn(CF_3SO_3)_2$	9.2	0.03	282	2.52	Toluene	60	111
$Zn(CF_3SO_3)_2$**	11.3	0.03	349	3.11	Toluene	66	111
$Zn(CF_3SO_3)_2$	12.5	0.03	383	3.43	Toluene	70	125
Zn/H-BEA	54.4	0.03	299	2.67	CH_3CN	60	82
Zn/H-BEA	65.5	0.03	359	3.21	Toluene	60	82
Zn/H-BEA	55.6	0.03	305	2.72	Toluene	60	95
Zn/H-BEA	56.0	0.03	307	2.74	Toluene	70	111
Zn/H-BEA	58.3	0.03	320	2.85	Toluene	65	125

*Seventy-μL, 0.79×10^{-3} mol.
**Fifty-five-μL, 0.62×10^{-3} mol CF_3SO_3H were added as cocatalyst to the reaction mixture.

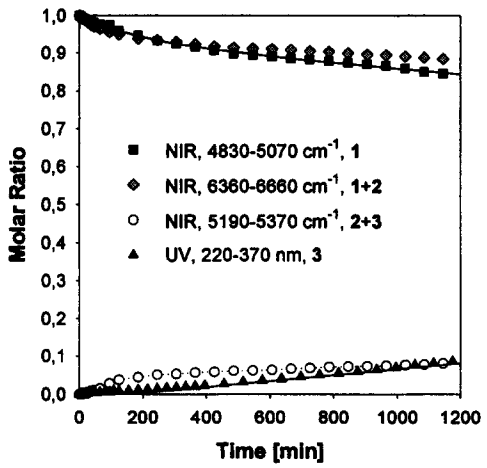

Figure 1. Change in concentration of 1 (NIR, 4,830–5,070 cm^{-1}) and 3 (UV, 220–370 nm) with time in the cyclization of 1 with $Zn(CF_3SO_3)_2$ (CH_3CN, 82°C, s/c 100).

The concentrations of 1 and 3 were fitted with the model (continuous lines), which allowed prediction of the concentration of the intermediate 2 (dashed line). From absorption bands at 6,519 and 5,264 cm^{-1}, the sum of the concentrations of compounds 1+2 and 2+3, respectively, was estimated.

remained lower than expected from the decrease in the concentration of **1**. The mass balance can, however, be closed by assuming that an intermediate species has formed in the reaction mixture. The enamine **2**, as postulated in the chemical equation, was tentatively assigned to this intermediate. In order to confirm the nature of the intermediate, the reaction was also followed *in situ* with ^{1}H-NMR spectroscopy (Su and Müller, 2002). Transient signals were observed at 3.40 and 3.24 ppm and assigned to the two chemically different methylene protons of **2**. This confirmed that the intermediate was 2-methyl-1,2-dehydropiperidine.

Closer inspection of the NIR spectra showed the presence of two further signals, which did not follow the increase or decrease of the other NIR peaks closely (Figure 1).

1. An intense band was observed at 5264 cm^{-1}. Integration in the 5190–5370-cm^{-1} region showed that its area initially increased in parallel with the decrease of the signals due to **1**. At reaction times between 400 and 800 min, the intensity of the signal was approximately constant. However, at very long reaction times, its intensity increased in parallel to the intensity of the absorption band arising from **3** in the UV region. Therefore, the band at 5264 cm^{-1} is assigned to the intermediate species, which is superimposed by an absorption band of **3**.

2. A peak with maximum intensity at 6519 cm^{-1} is generally observed for compounds containing either secondary or primary amine groups and is characteristic for the N–H stretch vibration (Buback and Vögele, 1993). Integration of this peak in the 6,360–6,660 cm^{-1} region showed that its intensity initially followed the peaks assigned to **1**; however, at longer reaction times the area decreased more slowly than that of the absorption bands due to **1**. Thus, the peak is tentatively attributed to a superimposition of absorption bands due to the NH_2-group in **1**, and the NH-group in **2**.

As neither the extinction coefficients nor the appropriate calibration mixtures for **2** were available, the absorption maxima at 5,264 and 6,519 cm^{-1} were not used for the quantitative analysis.

Mathematical modeling of the reaction

A mathematical model was developed to describe the course of the reaction and to derive the rate constants of each reaction step. The simplest model, involving an intermediate species, comprises two irreversible steps (Eq. 2)

$$S \xrightarrow{k_1} I \xrightarrow{k_2} P \tag{2}$$

Assuming first order in the substrate [when the concentration of the catalyst $Zn(CF_3SO_3)_2$ was held constant at 2.1×10^{-4} mol·dm^{-3} and the initial concentration of **1** varied in the range 1.8×10^{-2} mol·dm^{-3} to 8.8×10^{-2} mol·dm^{-3}, a double logarithmic plot of the initial rate vs. catalyst concentration indicated the reaction to be close to first order in **1**; an approximate first-order kinetics was also reported for the cyclization of **1** with $[Cu(CH_3CN)_4]PF_6$ (Müller et al., 2000)]; the change in concentration of the substrate with time can be described with the differential equation (Eq. 3). This equation can also be written in an integrated form (Eq. 4). In contrast, the concentrations of the intermediate and of the product are a more complex function with time

$$-\frac{d[S]}{dt} = k_1[S] \tag{3}$$

$$[S]_t = [S]_0 e^{-k_1 t} \tag{4}$$

According to this model, the concentration of the substrate would decrease exponentially with time. The decrease in the concentration of **1** observed was indeed close to the exponential decrease at low conversions (see parenthetical note following Eq. 2). However, the reaction deviated significantly from first-order kinetics at conversions above 10%. Therefore, a more advanced model was needed to describe the reaction, which was based on a reversible conversion of substrate **1** to the intermediate, followed by the irreversible reaction to the product **3** (Eq. 5)

$$S \underset{k_{-1}}{\overset{k_1}{\rightleftharpoons}} I \xrightarrow{k_2} P \tag{5}$$

The change in concentration of the substrate, the intermediate, and the product with time is then given by differential equations (Eqs. 6–8)

$$\frac{d[S]}{dt} = -k_1[S] + k_{-1}[I] \tag{6}$$

$$\frac{d[I]}{dt} = k_1[S] - k_{-1}[I] - k_2[I] \tag{7}$$

$$\frac{d[P]}{dt} = k_2[I] \tag{8}$$

The exact solution of these equations is known (Connors, 1990; Espenson, 1995), and is given in Eqs. 9–11

$$[S]_t = \frac{[S]_0}{\beta - \alpha}\{(k-\alpha)e^{-\alpha t} - (k-\beta)e^{-\beta t}\} \quad (9)$$

$$[I]_t = \frac{k_1[S]_0}{\beta - \alpha}e^{-\alpha t} - e^{-\beta t} \quad (10)$$

$$[P]_t = [S]_0\left(1 + \frac{\beta}{\alpha - \beta}e^{-\alpha t} - \frac{\alpha}{\alpha - \beta}e^{-\beta t}\right) \quad (11)$$

where $k = k_{-1} + k_2$, $\alpha\beta = k_1 k_2$, $\alpha + \beta = k_1 + k_{-1} + k_2$.

Using this set of equations, the parameters α, β, and k were fitted to the experimental data. First, the changes in the concentration of **1** and **3** were concurrently fitted with the model. As can be seen from Figure 1, the model can describe the observed concentrations for **1** and **3** well (continuous lines). Using the values for α, β, and k, the concentration of the intermediate was then predicted (dashed line). The intermediate reached a maximum concentration of ca. 6–8% after 6 h.

From the parameters α, β, and k, the respective rate constants, k_i, for the individual reaction steps were calculated ($k_1 = 0.41 \times 10^{-3}$, $k_{-1} = 3.62 \times 10^{-3}$, and $k_2 = 1.04 \times 10^{-3}$ min^{-1}). The slowest step in the reaction sequence was the formation of the intermediate. Both sequential reactions (back to **1** or forward to **3**) were faster than the formation of the intermediate, although the rate constants k_1, k_{-1}, and k_2 do not differ more than one order of magnitude. This is in line with the fact that the intermediate is formed in significant concentrations. The equilibrium constant K_{eq}, which formally describes the equilibrium between **1** and **2**, is on the side of the starting material ($K_{eq} = 0.11$). However, care has to be taken in the interpretation of K_{eq}, as the mathematical error is high, K_{eq} being calculated as the ratio of two small numbers. In the kinetic analysis, the concentration of the catalyst was not taken into account, as it was small relative to the substrate concentration and remained constant over the whole course of the reaction. Therefore, the rate constants, k_i, are effective rate constants, which have to be divided by the catalyst concentration to obtain the rate per metal center.

This sequence of reactions can be displayed in a reaction profile diagram using Eyring's transition-state theory to relate the rate constants with $\Delta G°$ (Connors, 1990). For the reaction-profile diagram, as shown in Figure 2, the free energy $\Delta G°$ of compound **1** was defined as zero. The intermediate had a slightly higher potential energy than **1** ($\Delta G° \approx 6$ $kJ \cdot mol^{-1}$ at 82°C), which is in agreement with related experimental data (Müller et al., 2002; Koch et al., 1999). The second reaction step seems to be effectively irreversible. In this respect, it is known that the equilibrium between enamines and imines is fully on the side of the imine (Ahlbrecht and Fischer, 1973; Lu and Lewin, 1998; Caccamese and Principato, 1998). Therefore, the potential energy of the product should be very low compared to the starting material and the intermediate. The reaction profile further indicates that the transition states of hydroamination and subsequent isomerization have approximately the same potential energy. Therefore, both reaction steps have to be taken into account for an appropriate kinetic description of the reaction.

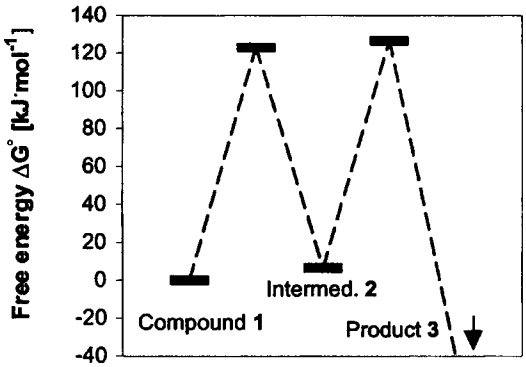

Figure 2. Reaction profile for cyclization of 1 with $Zn(CF_3SO_3)_2$ at 82°C in CH_3CN.
Compound 1: $\Delta G° \equiv 0$.

In some experiments, the cyclization of **1** was followed only with UV- and not with NIR-spectroscopy. In this case, only the formation of the product is reported. The change in the product concentration with time was adequately described by Eq. 11, but the individual rate constants were unavailable. However, it was possible to obtain the value of α and β, and to calculate k_{tot} as a measure for the rate of the overall process according to Eq. 12

$$k_{tot} = \frac{\alpha\beta}{\alpha + \beta} \quad (12)$$

This corresponds to an approximation of the reaction by the improved steady-state solution, which is valid when none of the reaction steps is rate controlling (McDaniel and Smoot, 1956).

Table 2. Rate Constants k_i Measured for the Cyclization of 1 with $Zn(CF_3SO_3)_2$

Solvent	Temp. [° C]	s/c	k_1 [10^{-3} min^{-1}]	k_{-1} [10^{-3} min^{-1}]	k_2 [10^{-3} min^{-1}]	k_{tot} [10^{-3} min^{-1}]
Toluene	82	100	0.24	0.46	0.88	0.13
Toluene	111	100	2.28	3.19	1.03	0.36
Toluene	125	100	5.15	7.21	1.93	0.70
CH_3CN	82	100	0.41	3.62	1.04	0.08
CH_3CN	82	10	1.35	6.03	0.97	0.16
CH_3CN	100	10	—	—	—	0.60
CH_3CN	110	10	—	—	—	0.91
CH_3CN	120	10	—	—	—	1.18

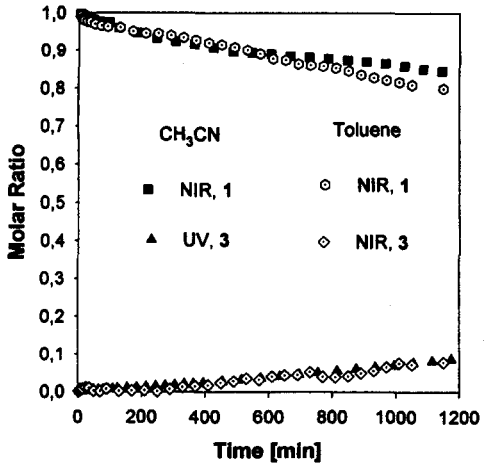

Figure 3. Comparison of CH_3CN and toluene as solvents in the cyclization of 1 with $Zn(CF_3SO_3)_2$ (82°C, s/c 100).

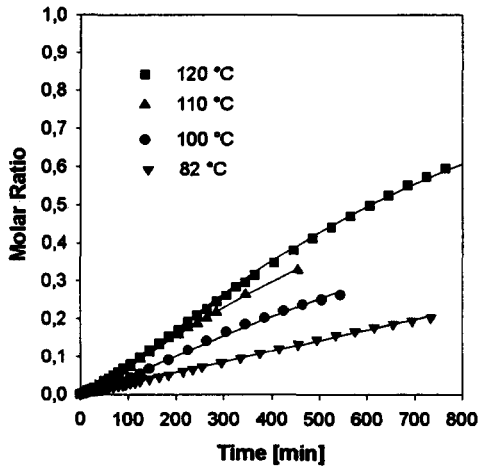

Figure 5. Increase in the concentration of 3 with time in the cyclization of 1 using the catalyst $Zn(CF_3SO_3)_2$ at various temperatures (UV, CH_3CN, s/c 10).

Hydroamination using $Zn(CF_3SO_3)_2$ as catalyst

To obtain further information on the rate law, the reaction was also performed using a 10-fold higher concentration of catalyst. The overall rate of reaction doubled from 0.08×10^{-3} to 0.16×10^{-3} min^{-1} upon a 10-fold increase in catalyst concentration [substrate to catalyst ratios (s/c), of 10 and 100, respectively, CH_3CN, 82°C]. The increase in rate was reflected in the higher rate constants, k_1 and k_{-1}, whereas the rate constant k_2 remained unchanged (Table 2). This suggests that only the hydroamination reaction is zinc catalyzed, whereas the isomerization of the enamine to the imine is not metal catalyzed. The latter becomes the rate-limiting step with increasing catalyst concentration. However, it cannot be excluded that the decreasing rate constant per unit catalyst is a result of nonkinetic effects.

Another important factor in homogeneous catalysis is the choice of solvent. In this respect, toluene had been described as an especially favorable solvent for hydroamination reactions (Müller et al., 2000), whereas CH_3CN was especially suitable for *in situ* spectroscopy. Therefore, the catalytic activity of $Zn(CF_3SO_3)_2$ for the cyclization of **1** was compared in these two solvents. At 82° C, the rate of reaction was very similar in toluene and CH_3CN (Figure 3). Closer inspection of the rate constants k_i showed that hydroamination and reverse hydroamination were faster in CH_3CN, whereas the subsequent isomerization of the enamine to the imine had approximately the same reaction rate in both solvents (Table 2). This suggests that the more polar solvent CH_3CN stabilizes a polar transition state in the hydroamination reaction (Marcus, 1999). However, the higher reaction rate is compensated by a shift of the hydroamination equilibrium toward the starting aminoalkyne. Because of the two opposing effects, the overall rate is very similar in the two solvents.

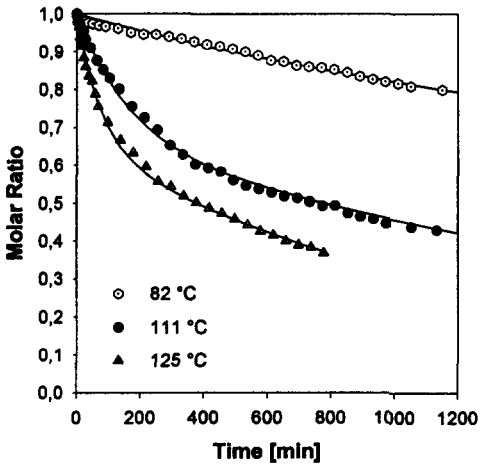

Figure 4. Comparison of different reaction temperatures in the cyclization of 1 with $Zn(CF_3SO_3)_2$ (NIR, toluene, s/c 100).

A more complete picture is obtained when the temperature dependence of the reaction in the two solvents is considered. In toluene, the overall rate of reaction (k_{tot}) increased from 0.13×10^{-3} min^{-1} to 0.70×10^{-3} min^{-1} upon an increase in temperature from 82°C to 125°C (Figure 4 for s/c = 100). In CH_3CN, the rate of reaction increased from 0.16×10^{-3} min^{-1} to 1.18×10^{-3} min^{-1} upon an increase in temperature from 82° to 120°C (Figure 5 for s/c = 10). Thus, the temperature dependence of the overall reaction was very similar in the two solvents. The different ratio of substrate to catalyst in the two sets of experiments is probably of minor importance, as the reaction seems not to be diffusion or equilibrium limited. The apparent activation energies were 44 and 41 $kJ\cdot mol^{-1}$ in toluene and CH_3CN, respectively, reflecting the small difference in temperature dependence in the two solvents. Closer inspection of the rate constants, k_i, showed that, in toluene, the constants k_1 and k_{-1} increased in parallel and had a higher temperature dependence than k_2 (Table 2). The equilibrium constant K_{eq} for the hydroamination step was constant in the temperature range from 82°C to 125°C within the experimental error. This indicates a very small enthalpy $\Delta H°$ for this reaction step. In principle, the enthalpy

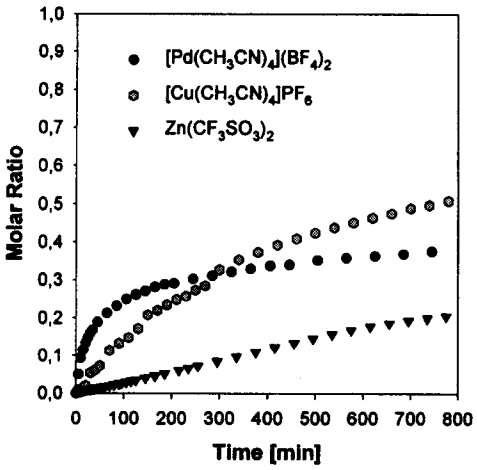

Figure 6. Increase in the concentration of 3 with time using different catalysts (UV, CH_3CN, 82°C, s /c 10).

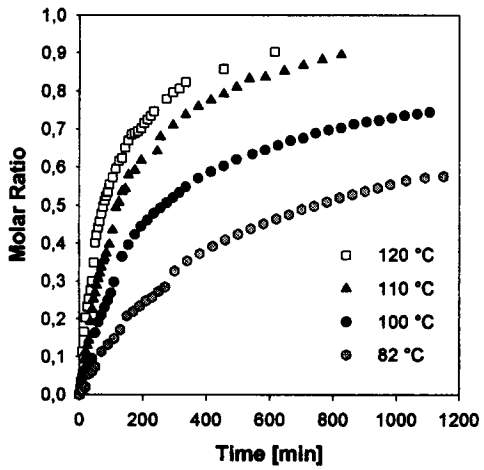

Figure 7. Increase in the concentration of 3 with time using the catalyst $[Cu(CH_3CN)_4]PF_6$ at different temperatures (UV, CH_3CN, s/c 10).

of the reaction can be estimated from the difference between the apparent activation energies of the forward and reverse reactions. Using the Arrhenius equation, the difference between the activation energy of the hydroamination and the reverse reaction is calculated to be 9.6 $kJ \cdot mol^{-1}$. This confirms that the reaction enthalpy for the reaction of **1** to **2** is small.

Lewis acidic metal catalysts other than $Zn(CF_3SO_3)_2$

The reaction rate was also measured for the catalysts based on Lewis acidic complexes of copper(I) and palladium(II) (Figure 6 and Table 3). In CH_3CN(82°C), the catalytic activity of $[Cu(CH_3CN)_4]PF_6$ ($k_{tot} = 1.13 \times 10^{-3}$ min^{-1}) was about seven times higher than that of $Zn(CF_3SO_3)_2$ ($k_{tot} = 0.16 \times 10^{-3}$ min^{-1}). The catalytic activity of the copper complex increased at higher temperatures (Figure 7); however, at longer reaction times the observed product concentration was significantly lower than calculated from the model. This could either be the result of deactivation of the copper catalyst or indicate a different reaction mechanism.

At short reaction times, the catalytic activity of $[Pd(CH_3CN)_4](BF_4)_2$ was even higher (Figure 6). During the first 30 min of the reaction, this catalyst was about 200 times more active than $Zn(CF_3SO_3)_2$ ($k_{tot} \approx 7.95 \times 10^{-3}$ min^{-1} at 82°C). However, the high initial activity of the catalyst diminished quickly, and the catalyst apparently became deactivated. This effect was more pronounced at higher temperatures, although a higher conversion was achieved (Figure 8). After the reaction, the product mixtures were black, probably because the palladium complex had decomposed to metallic palladium. In this respect, it is known that many palladium(II) complexes are not stable in a solution without a protecting sphere of strongly coordinating ligands, like phosphanes (Collman et al., 1987). The solvent acetonitrile also coordinates to a palladium, but the interaction is weak and, apparently, cannot stabilize the palladium in the oxidation state + 2 sufficiently.

In order to test the activity of a palladium complex stabilized by a ligand sphere, $[Pd(Triphos)](CF_3SO_3)_2$, Triphos = *bis*-(diphenylphosphinoethyl)-phenylphosphane was tested as a catalyst. The geometry of the complex is based on the typical square planar coordination sphere of palladium(II) (Müller et al., 2001). Three of the coordination sites are occupied by phosphane ligands, and the fourth is available for binding the substrate. A lower initial activity of $[Pd(Triphos)](CF_3SO_3)_2$, in the cyclization of **1**, was compensated by a higher stability in comparison to $[Pd(CH_3CN)_4](BF_4)_2$. Therefore, it was possible to achieve full conversion with this catalyst. Upon an increase in temperature from 82°C to 120°C, the overall rate constant increased from 0.20×10^{-3} to 0.70×10^{-3} min^{-1} (Table 3).

Table 3. Temperature Dependence of Rate Constants k_i Measured for the Cyclization of 1 with $[Pd(Triphos)](CF_3SO_3)_2$ and $[Cu(CH_3CN)_4]PF_6$ (Solvent CH_3CN)

Catalyst	Temp. [° C]	s/c	k_1 [10^{-3} min^{-1}]	k_{-1} [10^{-3} min^{-1}]	k_2 [10^{-3} min^{-1}]	k_{tot} [10^{-3} min^{-1}]
$[Pd(Triphos)](CF_3SO_3)_2$	82	100	0.54	5.06	3.37	0.20
$[Pd(Triphos)](CF_3SO_3)_2$	100	100	1.42	5.16	2.92	0.44
$[Pd(Triphos)](CF_3SO_3)_2$	120	100	2.44	5.26	3.09	0.70
$[Cu(CH_3CN)_4]PF_6$	82	10	—	—	—	1.13
$[Cu(CH_3CN)_4]PF_6$	100	10	—	—	—	3.04
$[Cu(CH_3CN)_4]PF_6$	110	10	—	—	—	7.15
$[Cu(CH_3CN)_4]PF_6$	120	10	—	—	—	11.2

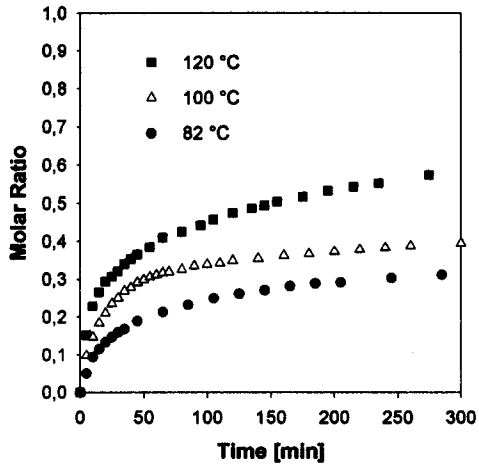

Figure 8. Increase in the concentration of 3 with time using the catalyst $[Pd(CH_3CN)_4](BF_4)_2$ at different temperatures (UV, CH_3CN, s/c 10).

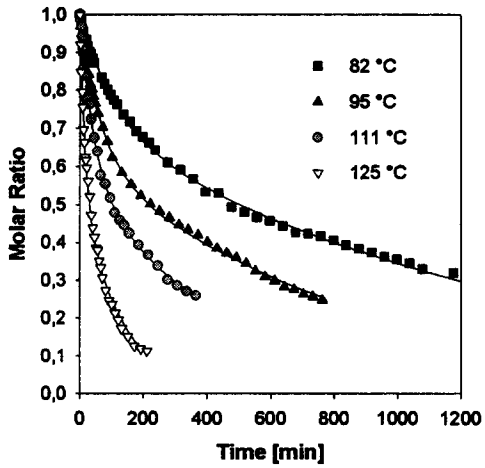

Figure 10. Decrease in the concentration of 1 with time using the catalyst Zn/H-BEA at different temperatures (NIR, toluene, s/c 100).

Similar to the zinc catalyst, the increase was due to a higher k_1 (and k_{-1}) at elevated temperatures.

Heterogeneous catalysis with Zn/H-BEA

The corresponding heterogeneous catalyst, Zn/H-BEA zeolite, suspended in toluene, was employed as catalyst in the cyclization of **1** and the reaction followed by NIR-spectroscopy (Figure 9). From integration of the spectra in the regions 4,910 to 5,045 cm^{-1} and 5,205 to 5,345 cm^{-1}, the concentrations of **1** and **3** were determined, respectively. The cyclization of **1** with Zn/H-BEA was very fast and, at 125°C, was the fastest reaction described in this study. As was observed in homogeneous catalysis, the concentration of **1** decreased immediately from the start of the reaction, whereas **3** was formed with an initial time delay. Thus, an intermediate species must have formed when Zn/H-BEA was employed as the catalyst. It was, therefore, tested whether the kinetic model developed for the homogeneous catalysis was also valid for the heterogeneous catalysis. After fitting the variables α, β, and k to the experimental data, a very good match between calculated and experimental concentrations was obtained (Figure 9). Thus, the same kinetic model can be used to describe the homogeneously and the heterogeneously catalyzed reactions. This indicates that, in the case of the heterogeneous reaction, the rate of reaction is limited by the catalytic process at the metal center, whereas intraporous or external diffusion had little influence on the overall rate of reaction (Chen et al., 1994).

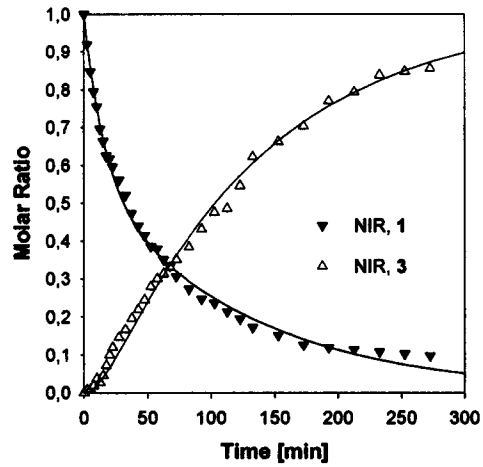

Figure 9. Concentrations of 1 and 3 measured (points) and calculated from the model (lines) in the cyclization of 1 with Zn/H-BEA (NIR, toluene, 125°C, s/c 100).

The catalytic activity of Zn/H-BEA was strongly dependent on the temperature. Upon an increase in temperature from 82°C to 125°C, the overall rate constant, k_{tot}, increased from 0.68×10^{-3} min^{-1} to 7.15×10^{-3} min^{-1} (Figure 10). This corresponds to an activation energy of 62 $kJ\cdot mol^{-1}$. The high overall reaction rate at 125°C was due to high values for k_1, k_{-1}, and k_2 (31.9×10^{-3}, 23.3×10^{-3} and 15.9×10^{-3} min^{-1}, respectively).

Under the same reaction conditions, Zn/H-BEA had a higher catalytic activity than the corresponding homogeneous catalyst $Zn(CF_3SO_3)_2$ (Figures 11a, 11b, and Table 4). In toluene at 111°C, the rate constants of all reaction steps were three to five times higher for Zn/H-BEA than for $Zn(CF_3SO_3)_2$. Thus, the heterogeneous catalyst is more active in both hydroamination and isomerization. There are two possible explanations: (1) the substrate becomes concentrated on the surface of the zeolite by reversible adsorption. The adsorption site might be a Lewis acid/Brønsted acid site pair so that coordination of the alkyne to the metal center is accompanied by protonation of the amine group. Hydroamination and isomerization may be favored by this pathway, which involves the protonated metal–substrate complex as an intermediate. (2) Since the isomerization of the enamine to the imine is not catalyzed by the zinc ions as shown for the homogeneous catalyst $Zn(CF_3SO_3)_2$, protons remaining in the BEA zeolite after the ion exchange could function as cocatalyst. In this respect, it is known that the isomerization of enamines to the corresponding imines can be catalyzed by Brønsted acids (Stanforth, 2001). To test the hypothesis, CF_3SO_3H (20 equivalents relative to Zn^{2+}) was added to a

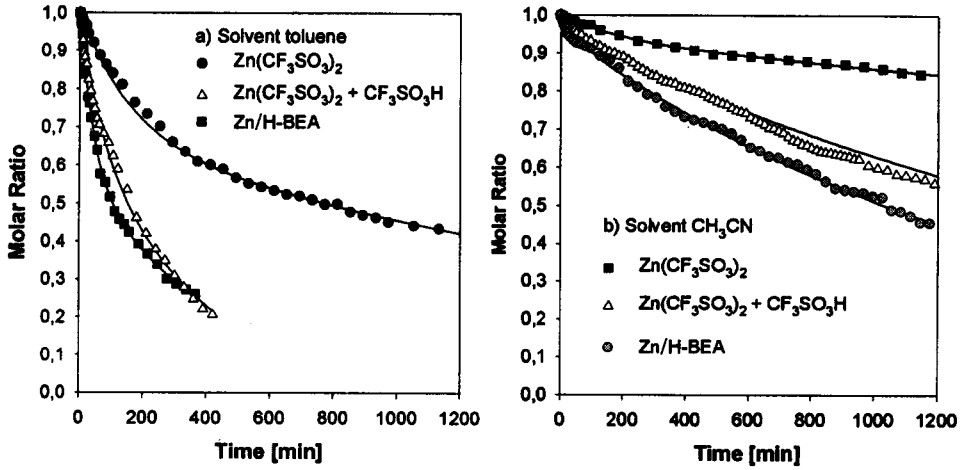

Figure 11. Decrease in the concentration of 1 with time using the heterogeneous catalyst Zn/H-BEA, the homogeneous catalyst $Zn(CF_3SO_3)_2$, and $Zn(CF_3SO_3)_2$ in the presence of a 20-fold molar excess of CF_3SO_3H.

The solvents used were (a) toluene (111°C, NIR, s/c 100) and (b) CH_3CN (82°C, NIR, s/c 100).

Table 4. Rate Constants for the Cyclization of 1 with Zn/H-BEA Compared to Homogeneous Catalysts (s/c 100)

Catalyst	Temp. [° C]	k_1 [10^{-3} min^{-1}]	k_{-1} [10^{-3} min^{-1}]	k_2 [10^{-3} min^{-1}]	k_{tot} [10^{-3} min^{-1}]
Solvent toluene					
$Zn(CF_3SO_3)_2$	111	2.28	3.19	1.03	0.36
$Zn(CF_3SO_3)_2$, CF_3SO_3H	111	6.30	5.45	7.84	2.52
Zn/H-BEA	82	3.07	4.56	2.18	0.68
Zn/H-BEA	95	6.50	7.46	2.85	1.10
Zn/H-BEA	111	10.7	9.23	4.71	2.04
Zn/H-BEA	125	31.9	23.3	15.9	7.15
Solvent CH_3CN					
$Zn(CF_3SO_3)_2$	82	0.41	3.62	1.04	0.08
$Zn(CF_3SO_3)_2$, CF_3SO_3H	82	0.97	6.52	5.28	0.40
Zn/H-BEA	82	1.51	10.2	7.68	0.60

mixture of $Zn(CF_3SO_3)_2$ and **1** (Su and Müller, 2001). In toluene, the overall rate of reaction increased sharply from 0.36×10^{-3} min^{-1} to 2.52×10^{-3} min^{-1}. In CH_3CN, the rate of reaction increased from 0.08×10^{-3} min^{-1} to 0.40×10^{-3} min^{-1}. Whereas k_1 and k_{-1} doubled, an 8 (5)-fold increase in k_2 was observed. This clearly shows that the isomerization of **2** to **3** is catalyzed by protons. Additionally, the protons also function as cocatalysts in the hydroamination step (**1** to **2**). Thus, we postulate that a proton transfer step is involved in both reactions.

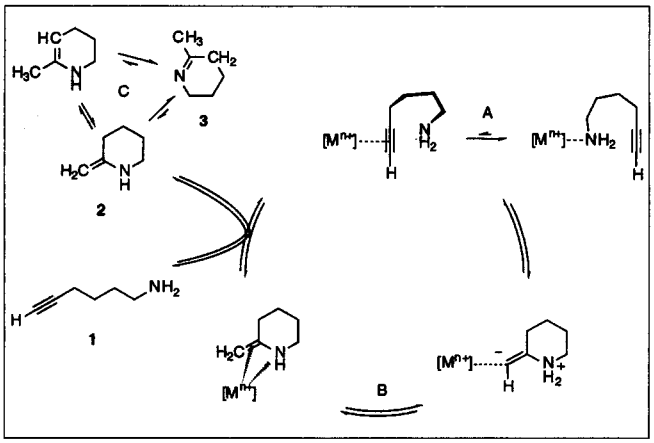

Figure 12. Reaction mechanism proposed for the cyclization of 1.

The proposed catalytic cycle is depicted in Figure 12. For successful catalysis, the reactant has to bind to the metal center. Despite the preference for attaching via the amine end of the molecule, some of the 6-aminohex-1-yne molecules are bound via the alkyne bond. The interaction of the alkyne with the metal center reduces the electron density in the π-system and allows the nucleophilic attack of the amine nitrogen atom at the secondary carbon atom of the CC triple bond (Collman et al., 1987). The intermediate 2-ammonio alkenyl complex formed in this way requires a proton for the protolytic cleavage of the metal–carbon bond. The enamine **2** is then released and isomerizes *in situ* to the corresponding imine **3**.

The protons are involved in three elementary steps, suggesting that the Brønsted and Lewis acid sites in close vicinity may be necessary in an ideal catalyst.

1. Because the amine group in **1** is the strongest base in the reaction mixture, added acids will protonate it *in situ* to

the ammonium salt, which has less of a tendency to bind to the metal center. Thus, the probability of coordination of the alkyne group to the metal center is increased in acidic reaction media.

2. The protolytic cleavage of the metal–carbon bond in the intermediate 2-ammonio alkenyl complex is facilitated in acidic conditions. The formal 1,3-hydrogen shift from the ammonium group to the α-carbon atom is, as a [1,3] sigmatropic rearrangement, orbital-forbidden (Fleming, 1976). A recent theoretical study confirmed that an intermolecular proton transfer was more likely (Senn et al., 2000). In this case, an additional proton acceptor, for example, the counterion or the solvent, can act as a proton shuttle.

3. The isomerization of **2** to **3** is accelerated in the presence of protons. If dissociation of **2** from the coordination sphere is slow, the lower transient concentration of **2** in acidic conditions would result in a higher overall rate of reaction.

Considering this reaction sequence, the rate constant k_2 describes a true elementary reaction step, whereas k_1 and k_{-1} constitute formal rate constants, describing the overall rate for the sequence of reaction steps leading from **1** to **2** and the reverse reaction, respectively.

Conclusion and Outlook

The cyclization of 6-aminohex-1-yne (**1**) was studied as a model reaction for the direct addition of amine N–H to CC multiple bonds (hydroamination). The product was the enamine 2-methylene-piperidine (**2**), which isomerized *in situ* to the corresponding imine 2-methyl-1,2-dehydropiperidine (**3**). The most active homogeneous catalyst for the cyclization of **1** was $[Pd(CH_3CN)_4](BF_4)_2$. However, the complex rapidly decomposed, most likely to a metallic palladium. Higher stability was observed for the corresponding phosphane complex $[Pd(Triphos)](CF_3SO_3)_2$. The phosphane coordinates to palladium in a tridentate fashion. The fourth site is available for binding of the substrate, allowing further catalytic action. Other Lewis acidic late transition metal complexes also catalyze the cyclization of **1**. The copper complex $[Cu(CH_3CN)_4]PF_6$ was catalytically more active than $[Pd(Triphos)](CF_3SO_3)_2$, whereas the zinc salt $Zn(CF_3SO_3)_2$ was less active.

The cyclization of **1** with $Zn(CF_3SO_3)_2$ is adequately described with a kinetic model based on a reversible hydroamination of **1**, followed by an effectively irreversible isomerization of **2** to **3**. Although this model successfully describes the cyclization of **1**, it may not necessarily apply to corresponding intermolecular reactions. For the cyclization of 6-aminohex-1-yne, it was shown that the former step (hydroamination) required the presence of a metal catalyst, whereas the latter step (enamine–imine isomerization) was catalyzed by protons. However, the metal-catalyzed hydroamination was also faster in acidic reaction conditions. The slowest step in the reaction sequence was the formation of **2**, whereas both reverse hydroamination of **2** to **1** and isomerization of **2** to **3** were faster. Since the rate of the three reaction steps did not differ more than one order of magnitude, significant concentrations of **2** were formed (6–8%).

Zn/H-BEA zeolite, employed as a heterogeneous catalyst, was significantly more active than the corresponding zinc salt $Zn(CF_3SO_3)_2$. The rate of both reaction steps, hydroamination and isomerization, was higher for Zn/H-BEA, which is probably due to the residual protons in the zeolite. Similarly, the catalytic activity of $Zn(CF_3SO_3)_2$ could be increased by the addition of a Brønsted acid (CF_3SO_3H) to the reaction mixture. Similar to the heterogeneous reaction, the rate of hydroamination and isomerization increased. This indicates that a proton transfer step is involved in both reaction steps. In summary, the simultaneous presence of a Brønsted and Lewis acid seems necessary for a fast and efficient catalysis of hydroamination reactions with late-transition metal compounds. Corresponding catalyst systems can be most efficiently realized with bifunctional solid materials, similar to the Zn/H-BEA zeolite used in this study, although liquid–liquid two-phase catalysis might also be possible (Neff et al., 2002).

Acknowledgments

The financial support of the *Deutsche Forschungsgemeinschaft* is gratefully acknowledged.

Literature Cited

Ahlbrecht, H., and S. Fischer, "Vinylamine-XIV; Untersuchungen zur Substituenten-Abhängigkeit der Imin-Enamin-Tautomerie an N-Aryl-vinylaminen," *Tetrahedron*, **29**, 659 (1973).

Arena, J. V., and T. M. Leu, "Deconvolution of Gas Chromatograms with Excel," *J. Chem. Educ.*, **76**, 867 (1999).

Buback, M., and H. P. Vögele, *FT-NIR Atlas*, VCH Verlagsgesellschaft, Weinheim (1993).

Caccamese, S., and G. Principato, "Resolution of the Enantiomers of Tetrahydrozoline by Chiral HPLC. The Racemization of the Enantiomers via an Imine-Enamine Tautomerism," *Tetrahedron Asymmetry*, **9**, 2939 (1998).

Cacchi, S., V. Carnicelli, and F. Marinelli, "Palladium-Catalysed Cyclization of 2-Alkynylanilines to 2-Substituted Indoles Under an Acidic Two-Phase System," *J. Organomet. Chem.*, **475**, 289 (1994).

Chen, N. Y., T. F. Degnan, and C. M. Smith, *Molecular Transport and Reaction in Zeolites*, VCH, New York (1994).

Collman, J. P., L. S. Hegedus, J. R. Norton, and R. G. Finke, *Principles and Applications of Organotransition Metal Chemistry*, Chs. 3, 4, 7, University Science Books, Mill Valley, CA, p. 66, 241, 409 (1987).

Connors, K. A., *Chemical Kinetics—The Study of Reaction Rates in Solution*, VCH, New York, p. 87 (1990).

Espenson, J. H., *Chemical Kinetics and Reaction Mechanisms*, 2 ed., McGraw-Hill, New York, pp. 77 and 86 (1995).

Fleming, I., *Frontier Orbitals and Organic Chemical Reactions*, Wiley, Chichester, p. 99 (1976).

Gottlieb, H. E., V. Kotlyar, and A. Nudelman, "NMR Chemical Shifts of Common Laboratory Solvents as Trace Impurities," *J. Org. Chem.*, **62**, 7512 (1997).

Hölderich, W. F., and G. Heitmann, "Synthesis of Intermediate and Fine Chemicals on Heterogeneous Catalysts with Respect to Environmental Protection," *Catal. Today*, **38**, 227 (1997).

Koch, H. F., L. A. Girard, and D. M. Roundhill, "Addition of Water and Ammonia to the Carbon-Carbon Double Bond of Acyclic Alkenes and Strained Bicyclic Dienes; A Computational Study," *Polyhedron*, **18**, 2275 (1999).

Lequitte, M., F. Figueras, C. Moreau, and S. Hub, "Amination of Butenes over Protonic Zeolites," *J. Catal.*, **163**, 255 (1996).

Li, Y., and T. J. Marks, "Organolanthanide-Catalyzed Intramolecular Hydroamination/Cyclization of Aminoalkynes," *J. Amer. Chem. Soc.*, **118**, 9295 (1996).

Lu, S.-P., and A. H. Lewin, "Enamine/Imine Tautomerism in α,β-Unsaturated-α-Amino Acids," *Tetrahedron*, **54**, 15097 (1998).

Marcus, Y., *The Properties of Solvents*, Vol. 4, P. G. T. Fogg, ed., Wiley, Chichester, pp. 55 and 187 (1999).

Table A1. Excel Worksheet

Column A	This column contains the time values in rows 2 to n.
Column B	This column contains the corresponding concentrations for **1** in rows 2 to n.
Column C	This column contains the corresponding concentrations for **3** in rows 2 to n.
Column D	= 1/(G$3-G$2)*((G$4-G$2)* EXP(-G$2*Am)-(G$4-G$3)* EXP(-G$3*Am))
Column E	= G$5/(G$3-G$2)*(EXP(-G$2*Am)-EXP(-G$3*Am))
Column F	= 1+(G$3/(G$2-G$3))* EXP(-G$2*Am)-(G$2/(G$2-G$3))* EXP(-G$3*Am)
Cell G1	= SUMXMY2(B2:Bn;D2:Dn)+SUMXMY2(C2:Cn;F2:Fn)
Cell G2 to G4	These cells contain the values of the parameters α, β, and k, respectively.
Cell G5	= G2+G3-G4
Cell G6	= G4-G7
Cell G7	= (G2* G3)/G5

Note: In the formulas given, m represents the row designation in the cell address that must be specified for each row in the actual worksheet ($2 \leq m \leq n$).

McDaniel, D. H., and C. R. Smoot, "Approximations in the Kinetics of Consecutive Reactions," *J. Phys. Chem.*, **60**, 966 (1956).

Mizuno, N., M. Tabata, T. Uematsu, and M. Iwamoto, "Amination of 2-Methylpropene over Proton-Exchanged ZSM-5 Zeolite Catalysts," *J. Catal.*, **146**, 249 (1994).

Müller, T. E., and A.-K. Pleier, "Intramolecular Hydroamination of Alkynes Catalysed by Late Transition Metals," *J. Chem. Soc., Dalton Trans.*, **4**, 583 (1998).

Müller, T. E., and M. Beller, "Metal-Initiated Amination of Alkenes and Alkynes," *Chem. Rev.*, **98**, 675 (1998).

Müller, T. E., M. Berger, M. Grosche, E. Herdtweck, and F. P. Schmidtchen, "Palladium-Catalyzed Cyclization of 6-Aminohex-1-yne," *Organometallics*, **20**, 4384 (2001).

Müller, T. E., M. Grosche, E. Herdtweck, A.-K. Pleier, E. Walter, and Y.-K. Yan, "Developing Transition-Metal Catalysts for the Intramolecular Hydroamination of Alkynes," *Organometallics*, **19**, 170 (2000).

Müller, T. E., "Hydroamination—Section D, Heterogeneous," *Encyclopedia of Catalysis*, I. T. Horváth, ed., Wiley, New York (2002).

Neale, R. S., L. Elek, and R. E. Malz, "The Zeolite-Catalyzed Amination of Acetylenes," *J. Catal.*, **27**, 432 (1972).

Neff, V., T. E. Müller, and J. A. Lercher, "Continuous Hydroamination in a Liquid–Liquid Two-Phase System," *J. Chem. Soc., Chem. Commun.*, **8906** (2002).

OPUS, 1997–2000, Bruker Optik GmbH, Version 3.1 (2000).

Penzien, J., T. E. Müller, and J. A. Lercher, "Zinc-Ion Exchanged Zeolites for the Intramolecular Hydroamination of 6-Aminohex-1-yne," *J. Chem. Soc., Chem. Commun.*, **18**, 1753 (2000).

Penzien, J., T. E. Müller, and J. A. Lercher, "Hydroamination of 6-Aminohex-1-yne over Zinc Based Homogeneous and Zeolite Catalysts," *Micropor. Mesopor. Mater.*, **48**, 285 (2001).

Roundhill, D. M., "Transition Metal and Enzyme Catalyzed Reactions Involving Reactions with Ammonia and Amines," *Chem. Rev.*, **92**, 1 (1992).

Senn, H. M., P. E. Blöchl, and A. Togni, "Toward an Alkene Hydroamination Catalyst: Static and Dynamic ab Initio DFT Studies," *J. Amer. Chem. Soc.*, **122**, 4098 (2000).

Stanforth, S. P., "The Wittig Reaction of Fluorinated Amides: Formation of Enamine and Imine Tautomers," *Tetrahedron*, **57**, 1833 (2001).

Su, R. Q., and T. E. Müller, "Co-Catalysis Between M^{n+} and H^+ in the Direct Addition of N–H Bonds to CC Double and Triple Bonds," *Tetrahedron*, **57**, 9431 (2001).

Su, R. Q., and T. E. Müller, "On the Direct Addition of Amine N–H to C ≡ C Triple Bonds with Late Transition Metal Catalysts," *Top. Catal.* (2002).

Tanabe, K., and W. F. Hölderich, "Industrial Application of Solid Acid-Base Catalysts," *Appl. Catal. A: Gen.*, **181**, 399 (1999).

Van Nhu, N., A. Wanner, H. Tiltscher, and J. A. Lercher, "On the Interfacial Mass Transfer and the Location of the Chemical Reaction in a Fluid/Fluid Reacting System at Elevated Temperatures and Pressures," *Catal. Today*, **66**, 335 (2001).

Table A2. Settings Used in Solver

Set target cell	$G$1
Equal to	Min
By changing cells	$G$2:$G$4
Solver Options	
Max. time	100 s
Iterations	100
Precision	0.000001
Tolerance	5%
Convergence	0.0001
Estimates	Tangent
Derivatives	Forward
Search	Newton

Appendix

Excel was employed to perform the nonlinear regression analysis. Table A1 provides an outline of the Excel worksheet for calculation of the kinetic data using the functions given in Eqs. 9–11. Columns B and C contain the concentrations of compounds **1** and **3** measured at the times given in column A. Columns D to F initially contain estimated values for the concentrations of compounds **1**, **2**, and **3**, which are calculated from the parameters α, β, and k, as given in G2 to G4. G1 gives the sum of the squares of the residuals, which is minimized in nonlinear regression analysis. The values of the rate constants k_1, k_{-1}, and k_2 are derived in G5 to G7.

For a given catalytic run, once the base-line corrected data are put in columns A to C of the worksheet and the initial estimates of the parameters entered in cells G2 to G4, nonlinear regression analysis can be performed. The solver module was used to optimize the values in cells G2 to G4 to obtain the minimum value in cell G1. This corresponds to the best fit of the calculated to the experimental data. The settings for the solver that were used to perform the nonlinear regression analysis are given in Table A2. Note that the target cell G1 represents the sum of the squares of the residuals, which is minimized to obtain the best fit of the equations that describes the data to the experimental data. In the worksheet, cells G2 to G4 contain the parameters that are systematically adjusted by the solver until the value in the target cell is minimized.

Manuscript received Dec. 6, 2001, and revision received June 12, 2002.